**Annuaire de l'Université de Sofia "St. Kliment Ohridski", Faculté de Physique, 96, 2003**

# ANALYSIS OF THE CLUSTER RESPONCE FUNCTION AND EUROBALL EFFICIENCY

STEPHANE LALKOVSKI, ANI MINKOVA, STOYANKA ILIEVA

*Department of Atomic Physics*

*Стефан Лалковски, Ани Минкова, Стоянка Илиева* АНАЛИЗ НА ФУНКЦИЯТА НА ОТКЛИК НА КЛЪСТЕР ДЕТЕКТОР И ЕФЕКТИВНОСТ НА EUROBALL

Статията е посветена на една от най-големите многодетекторни системи за $\gamma$-спектроскопия EUROBALL IV състояща се от 239 HP комптъново потиснати Ge детектори. 105 от тях са групирани по 7 в съставните клъстер детектори. В настоящата работа е представено експериментално изследване на функцията на отклик на клъстер детектора. Целта е да се определят оптималните условия за възстановяване на пълната енергия на детектиран $\gamma$-квант.

*Stephane Lalkovski, Ani Minkova, Stoyanka Ilieva.* ANALYSIS OF THE CLUSTER RESPONCE FUNCTION AND EUROBALL EFFICIENCY

This article is dedicated to the largest, at the present, $\gamma$-ray multidetector array EUROBALL IV, which consists of 239 high-pure anti-Compton shielded Ge detectors. 105 of them are grouped by 7, forming the so called "cluster" composite detector. Here we represent an experimental study of cluster's response functions. The aim is to determine the optimal conditions for detecting of the full $\gamma$-ray energy.

***Keywords:*** gamma spectroscopy; multidetectors; cluster and clover detectors

***PACS number:*** 26.20.Lv; 23.40.-s; 27.40.+z (A=56); 27.50.+e(A=60); 29.30.Kv

## INTRODUCTION

In the last decade the $\gamma$-ray spectroscopy has been essentially improved by introduction of a new generation multidetectors of $4\pi$ geometry. Several large $\gamma$-spectrometers as GASP, EUROGAM II, EUROBALL III and IV and GAMMASPHERE have been built. These arrays have been developed to study rare events connected with the nuclear structure at high-spin and many new phenomena have been observed.

The modern $\gamma$ detector arrays consists of many Ge detectors surrounded by a scintilator detector to detect and reject scattered radiation from the Ge crystal.

Thus the anticompton shield improve the P/T ratio. The multidetector arrays with composite detectors have an additional advantage—the add-back procedure which increases the detector efficiency at high energies. Here we represent an experimental study of the composite detector named "cluster" using $^{60}$Co and $^{56}$Co sources. The aim is to determine the optimal conditions for restoring the full $\gamma$-ray energy.

The article is organized as follows. The section 2 represents the main features of the interaction of $\gamma$-rays with matter. Section 3 gives some ratios for estimation of the detector quality. Section 4 describes the idea for effective Compton subtraction which takes place in all modern $\gamma$-ray detectors. The clover and cluster detectors are described in section 5. The main advantage of these detectors is increased photopeak efficiency, due to the add-back procedure, which is presented in section 6. The EUROBALL IV multidetector $\gamma$-ray array is presented in the next section 7. An experimental study of the cluster's response functions is presented in section 8. The total efficiency of EUROBALL IV is given in the section 9.

## 1. INTERACTION OF PHOTONS WITH MATTER

Gamma-rays interact with matter through three processes: photoeffect absorption, Compton scattering, and pair production, in which charged particles are liberated [1, 2]. These charged particles carry off the information about the $\gamma$-ray.

### PHOTOEFFECT

The *photoeffect* is a process in which an atom absorbs a photon and one of the atomic electrons is released. Free electron cannot absorb a photon because of the moment conservation, therefore only bounded electrons participate in the photoeffect. The electron kinetic energy $T_e$ is $T_e = E_\gamma - B_e$, where $E_\gamma$ is the photon energy and $B_e$—the electron binding energy.

Thus, the photoeffect is a liberation of an electron, which carries off most of the $\gamma$-ray energy, together with one or more low-energy electrons corresponding to the absorption of electron binding energy. If nothing escapes from the detector volume the sum of kinetic energies of all created electrons is equal to the original $\gamma$-ray energy.

The probability for photo-absorption of photons rapidly increases with the atomic number $Z$ (roughly as $Z^4$) and decreases with photon energy ($\sim E_\gamma{}^{-3}$). The $\gamma$-rays are fully absorbed in this process and their total energy is deposited in the detector.

### COMPTON EFFECT

The Compton effect is a process of inelastic scattering of photon with a nearly free atomic electron. The original photon energy is shared between the scattered photon and this ejected electron. If it is considered as free and initially at rest the conservation of linear momentum and total energy (using relativistic kinematics in the interaction plane) gives:

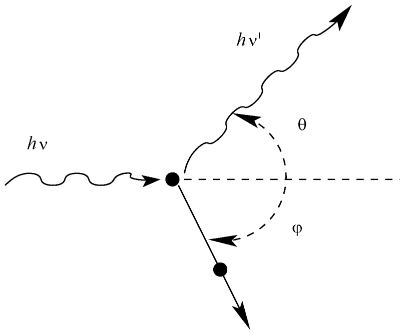


Fig. 1. Compton scattering kinematics

$$\frac{E_\gamma}{c} = \frac{E'_\gamma}{c}\cos\theta + \frac{m_0 c\beta}{\sqrt{1-\beta^2}}\cos\varphi \ , \tag{1}$$

$$0 = \frac{E'_\gamma}{c}\sin\theta - \frac{m_0 c\beta}{\sqrt{1-\beta^2}}\sin\varphi \ , \tag{2}$$

$$E_\gamma + m_0 c^2 = E'_\gamma + \frac{m_0 c^2}{\sqrt{1-\beta^2}} \ , \tag{3}$$

where $\beta = v/c$ is the electron velocity. Here $E_\gamma$ is the initial photon energy, $E'_\gamma$ is the Compton scattered photon energy, and the meaning of angles $\theta$ and $\varphi$ is clear from Fig. 1, giving a schematic view of the Compton process. Eliminating the unobserved variables $\varphi$ and $\beta$ the following equation for the scattered photon energy is obtained:

$$E'_\gamma = \frac{E_\gamma}{1+\alpha(1-\cos\theta)}. \tag{4}$$

The recoil Compton electron kinetic energy is

$$E_e = h\nu - h\nu' = h\nu\frac{\alpha(1-\cos\theta)}{1+\alpha(1-\cos\theta)} \tag{5}$$

where $\alpha = E_\gamma/m_0c^2$ is the photon energy in electron rest mass units. Two extreme cases can be distinguished.

1. The case of $\theta \cong 0$: It follows from eqs. (4) and (5) that $h\nu \cong h\nu'$ and $E_e \cong 0$. The recoil Compton electron has very low energy and the scattered $\gamma$-ray has energy close to that of the incident $\gamma$-ray.

2. A head-on collision in which $\theta = \pi$. In this case the incident $\gamma$-ray is scattered backward to its initial direction and the Compton electron recoils along the initial photon direction. In this extreme case the Compton electron has the maximum possible energy that can be transferred in a single Compton interaction. Eqs. (4) and (5) yield for this case

$$h\nu'|_{\theta=\pi} = \frac{h\nu}{1+2\alpha} \ , \tag{6}$$

$$E_e|_{\theta=\pi} = h\nu \frac{2\alpha}{1+2\alpha} \ . \tag{7}$$

In normal conditions all scattering angles might occur in the detector. Therefore the Compton electrons have continuous spectrum of energies from zero to the maximum energy predicted by eq. (7). The gap between the end of this continuous distribution corresponding to the maximum Compton electron energy and the full absorption peak is given by

$$E_c \equiv h\nu - E_e|_{\theta=\pi} = \frac{h\nu}{1+2\alpha}. \tag{8}$$

If the initial $\gamma$-ray energy is high enough ($h\nu \gg m_0c^2$) this energy difference tends to a constant value $E_c \cong m_0c^2/2 \sim 0.256$ MeV

The angular distribution of the Compton scattered photons is given by Klein-Nishina formula [3]:

$$\frac{\mathrm{d}\sigma_c}{\mathrm{d}\Omega} = r_0^2 \frac{1}{(1+\alpha(1-\cos\theta))^3} (\frac{1+\cos\theta}{2})(1+\frac{\alpha^2(1-\cos\theta)^2}{(1+\cos^2\theta)(1+\alpha(1-\cos\theta))}). \tag{9}$$

Here $r_0 = e^2/m_0c^2$ is the classical electron radius.

A polar plot of the angular distribution of Compton scattered photons for different energies of the initial $\gamma$-rays is shown in Fig. 2. The angular distribution is nearly symmetric for very low energy but for energy range 100 keV–10 MeV it is strongly asymmetric: the Compton scattered photons "prefer" to go forward in the initial photon direction. The $\gamma$-ray energy decreases in the multicompton scattering process (eq. (4)) therefore the angular distribution becomes more symmetric (see Fig. 2). This fact is applied in practice in the design of the anti-Compton shielded spectrometers described below (in sections 3 and 4).

The total cross section for Compton electrons can be obtained from a similar equation as (9) by integration over the solid angle and the result is the following:

$$\sigma_e = 2\pi r_0^2 \{\frac{1+\alpha}{\alpha^2}[\frac{2(1+\alpha)}{1+2\alpha} - \frac{1}{\alpha}\ln(1+2\alpha)] + \frac{1}{2\alpha}\ln(1+2\alpha) - \frac{1+3\alpha}{(1+2\alpha)^2}\} \ . \tag{10}$$

The total cross section eq.(10) decreases as $E^{-1}$ which is much less than that for photo-absorption ($E^{-3}$).

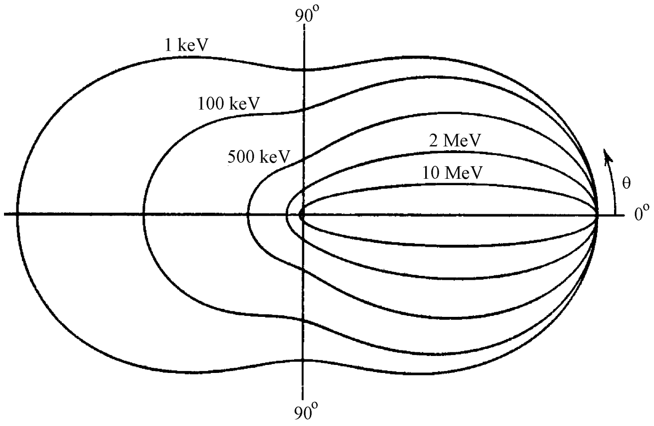


Fig. 2. Angular distribution of Compton scattered photons. The polar coordinates of each point of the angular distribution curve gives the scattering probability at angle $\theta$ (from [1])

## PAIR PRODUCTION

Pair production is another possible process for the interaction of photons with matter. In this process a high energy photon creates an electron-positron pair and the photon disappears. Obviously, a threshold of $2m_0c^2 = 1.022$ MeV exists for this process and, in general, pair production is important for high energy photons, becoming dominant for energies above 5 MeV.

The total energy conservation gives

$$E_\gamma = T_+ + m_0c^2 + T_- + m_0c^2 \ , \tag{11}$$

where $T_+$ and $T_-$ are the positron and electron kinetic energies, respectively. Just as in the case of photo-absorption, due to the momentum conservation this process is possible only in the vicinity of an atom. The recoil energy of this atom is neglected comparing to the other terms of eq.(11).

The positron slows down to energies close to the crystal electron energies. Then it annihilates with one crystal electron and two $\gamma$-rays of 511 keV appear. Both $\gamma$-rays might escape from the detector without interaction or might be totally or partially absorbed by Compton scattering. Therefore peaks at energy $E_\gamma - 2m_0c^2$ known as *double escape peak* and at energy $E_\gamma - m_0c^2$ known as *single escape peak* can appear together with the *full absorption peak* corresponding to $E_\gamma$.

## TOTAL CROSS SECTION

The total cross section ($\sigma$) for photon interaction with the matter is a sum of individual cross sections for photoeffect ($\sigma_p$), Compton scattering ($\sigma_c$), and pair production ($\sigma_{e^+e^-}$):

$$\sigma = \sigma_p + \sigma_c + \sigma_{e^+e^-} \,. \tag{12}$$

The contribution of each process in the total cross-section depends on the $\gamma$-ray energy and $Z$ of the absorber (see Fig. 3). Photons of energy $\leq 150$ keV interact in Ge crystal ($Z = 32$) mainly through photoeffect. The Compton scattering is dominant process for energies 150 keV $\leq E_\gamma \leq$ 8 MeV. Photons of energy higher than 8 MeV interact in Ge crystal mainly through pair production.

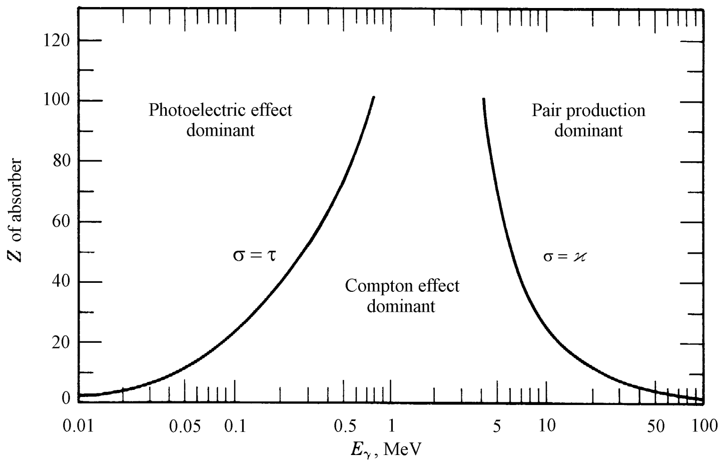


Fig. 3. The three $\gamma$-ray interaction processes and their regions of dominance [3]

## 2. GENERAL CHARACTERISTICS OF DETECTORS

The quality of a Ge detector depends on the efficiency, energy resolution, and peak-to-total ratio.

### EFFICIENCY

The *efficiency* of a single crystal is defined as a ratio of full-absorption peak counts, $N_{\rm ph}$ over the total number of photons, $N_\Omega$ emitted by the source in a solid angle $\Omega$ determined from the distance $r$ between the source and detector crystal surface and its area $S$ ($\Omega = S/r^2$).

$$\epsilon_p = \frac{N_{\rm ph}}{N_\Omega} \,. \tag{13}$$

The number of counts in the full-absorption peak depends on detector dimensions, therefore the efficiency of a single crystal depends on its diameter and

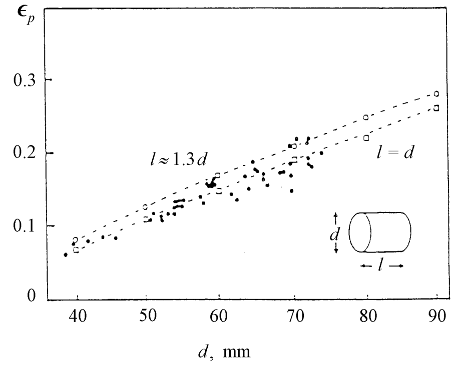


Fig. 4. Photopeak efficiency for a $\gamma$-ray of energy 1.33 MeV vs detector diameter. The Monte-Carlo simulation values are drawn by broken lines. Experimental values are with points (from [4])

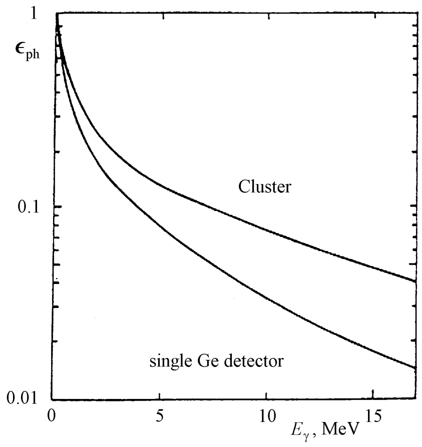


Fig. 5. Photopeak efficiency of a single Ge detector compared with a composite cluster detector which will be discussed later (from [5])

length. The crystal has to be long enough for the initial $\gamma$-rays to produce at least one interaction and its diameter $d$—large enough for the Compton-scattered $\gamma$-rays to stop inside the crystal. To determine the optimum ratio length/diameter Monte-Carlo simulations have been performed [4]. They show that a cylindrical detector of volume $V \geq 1000$ cm$^3$ has maximum efficiency at $l/d = 1.3$ for $\gamma$-rays of energy 1.17 and 1.33 MeV (Fig. 4). It was shown also that detector with $d \approx 80$ mm has $\epsilon_p$=0.25.

As the total cross section for $\gamma$-ray interaction with Ge crystal depends on the energy, the full-absorption peak will also depend on the energy. Monte-Carlo simulations (Fig. 5) show that the photopeak efficiency of a single Ge detector decreases rapidly with energy. To gain efficiency composite detectors have to be used. The efficiency of a composite detector, namely a cluster (see sec. 4) is presented in the same figure. Its efficiency is higher than that of a single Ge detector.

The *total efficiency* is the full-absorption peak counts divided by the total number of emitted photons, $N_{\rm em}$:

$$\epsilon_t = \frac{N_{\rm ph}}{N_{\rm em}}. \tag{14}$$

If we introduce the normalized solid angle $\omega = \Omega/4\pi$ the total efficiency is:

$$\epsilon_t = \epsilon_p \omega. \tag{15}$$

One can increase the total efficiency by increasing the solid angle. It can be obtained by building a spherical shell of close-packed Ge detectors.

*Relative efficiency* is the efficiency of a detector compared to a NaI scintillator reference detector of dimensions $d = 76.8$ mm and $l = 76.8$ mm.

$$(\epsilon_p\omega)_{\mathrm{rel}} = \frac{(\epsilon_p\omega)_{\mathrm{det}}}{(\epsilon_p\omega)_{\mathrm{NaI}}} \tag{16}$$

This NaI reference detector has an absolute efficiency of $1.2 \times 10^{-3}$ for a $\gamma$-ray of 1.33 MeV emitted by $^{60}$Co source placed at 25 cm from the detector.

## ENERGY RESOLUTION

The ability of a Ge detector to separate two $\gamma$-rays is given by its *energy resolution*. This is the extent to which the detector can distinguish two close $\gamma$-lines. The resolution is defined as *Full Width at Half Maximum (FWHM)* and it depends on the detector quality.

If a $\gamma$-ray with energy $E_\gamma$ creates $N$ pairs of carriers particle-hole $(p-h)$ then the following equation can be written:

$$E_\gamma = Nw, \tag{17}$$

where $w$ is the mean energy for $p-h$ creation. The statistic fluctuations of the number of created pairs is

$$\sigma(N) = 1/\sqrt{N}. \tag{18}$$

The energy fluctuations can be obtained from eqs.(17) and (18):

$$\sigma(E_\gamma) = \frac{E_\gamma}{\sqrt{N}} = w\sqrt{N}. \tag{19}$$

In first approximation the photopeak shape can be described by Gaussian function $G = \exp(-(x-x_0)^2/2\sigma^2)$.

The following expression can be obtained for $FWHM$:

$$FWHM = 2\sigma\sqrt{2\ln 2} = 2.35\sigma = 2.35E_\gamma/\sqrt{N} = 2.35\sqrt{E_\gamma w}. \tag{20}$$

Therefore the energy resolution depends on the $\gamma$-ray energy. The energy resolution for present Ge detectors is over 2.3 keV for a $\gamma$-ray of energy 1.33 MeV.

## DOPPLER EFFECT

When an excited nucleus moves with velocity $v$ the detected $\gamma$-ray energy $E$ is different from the emitted by a nucleus at rest $\gamma$-ray energy $E_0$. The *Doppler shifted* energy depends on the nucleus velocity and on the angle between the detector and the direction of the nucleus velocity $\theta$ (Fig. 6):

$$E(\theta) = E_0(1 + \beta\cos\theta), \tag{21}$$

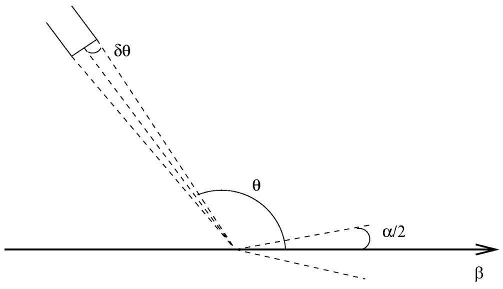


Fig. 6. Doppler effect

and the unshifted energy $E_0$ can be detected at angles $\theta = 90°$ and $\theta = 270°$.

The energy resolution defined by eq.(20) holds for $\gamma$-rays emitted by a stationary source, but it is degraded by Doppler effect if the $\gamma$-rays are emitted in flight.

The *Doppler broadening* of a $\gamma$-line is given by:

$$(\Delta E)_{\mathrm{Dopp}} = \sqrt{(\Delta E)^2_\theta + (\Delta E)^2_\alpha + (\Delta E)^2_\beta}\ , \tag{22}$$

where

$$(\Delta E)_\theta = E_0\beta \int_{\theta-\delta\theta}^{\theta+\delta\theta} \sin\theta \mathrm{d}\theta = 2E_0\beta \sin\theta \sin\delta\theta \tag{23}$$

is the Doppler broadening due to the opening angle $\delta\theta$ of the $\gamma$-ray detector.

$$(\Delta E)_\alpha = E_0\beta \int_{\theta-\frac{\alpha}{2}}^{\theta+\frac{\alpha}{2}} \sin\theta \mathrm{d}\theta = 2E_0\beta \sin\theta \sin\frac{\alpha}{2} \tag{24}$$

comes from the angular spread of the recoils, and

$$(\Delta E)_\beta = E_0 \int_0^{\delta\beta} \cos\theta \mathrm{d}\beta = E_0\beta\frac{\delta\beta}{\beta}\cos\theta \tag{25}$$

corresponds to the energy variation of the recoils.

There are different ways to reduce the Doppler broadening of the $\gamma$-lines.

• $\delta\theta$ (the detector opening) restriction. It can be achieved by detector segmentation or by construction of composite detectors.

• The second Doppler term can be controlled by means of ancillary detectors detecting the direction of the recoiling nuclei.

• $\delta\beta$ restriction. It is achieved by reducing the target thickness.

The total resolution $(\Delta E)_{\mathrm{tot}}$ will be worse than the detector intrinsic resolution $(\Delta E)_{\mathrm{in}}$ from eq.(20):

$$(\Delta E)_{\text{tot}} = \sqrt{(\Delta E)^2_{\text{in}} + (\Delta E)^2_{\text{Dopp}}}. \qquad (26)$$

The Doppler broadening expressed by the first term of eq.(22) has maximum value for detectors placed at about $90^0$ with respect to the beam direction ($\theta \approx 90^0$ and $\sin\theta \approx 1$).

The intrinsic resolution depends on the Ge detector and is typically 2 keV for $\gamma$-rays of energy 1.332 MeV, as it was mentioned above, so $(\Delta E)_{\text{in}}/E_0 \leq 0.002$. Typical values for $(\Delta E)_\theta/E_0$ are from 0.0048 to 0.07 at $\theta \approx 90^0$, $(\Delta E)_\alpha/E_0 \approx 0.003$ at $\theta \approx 90^0$, $(\Delta E)_\beta/E_0 \approx 0.003$ at $0^0$ [6]. One can deduce that for present $\gamma$-detector arrays the energy deterioration is dominated by the half-opening angle effect.

### PEAK-TO-TOTAL RATIO

The spectrum quality can be expressed by the *Peak-to-Total (P/T)* ratio defined as

$$P/T = \frac{N_{\text{peak}}}{N_{\text{tot}}}, \qquad (27)$$

where $N_{\text{peak}}$ is the full-absorption peak area and $N_{\text{tot}}$ is the total spectrum area. In case of two neighbouring peaks ($^{60}$Co) the definition (27) can be used and $N_{\text{peak}}$ has to be defined as a sum of the two full-absorption peaks. In case of multiple peaks spectra the (27) is incorrectly defined and it is better to use the following form:

$$P/B = \frac{N_{\text{peak}}}{N_{\text{bg}}}, \qquad (28)$$

where $N_{\text{bg}}$ is the background counts on the left peak side. The spectrum quality can be considerably improved by an escape-suppression (anti-Compton) shield surrounding the detector.

## 3. ESCAPE-SUPPRESSED SPECTROMETERS

The Compton scattering accounts for the major part of the $\gamma$-ray interactions in Ge crystals when the $\gamma$-ray energy is in the range 150 keV to 3 MeV. The multiple Compton scattering occurs with increasing of the $\gamma$-ray energy and it contributes to the detector full absorption peak for the large Ge detectors (Fig. 7). However the Compton-scattered $\gamma$-ray might survive without interaction and it could pass through the crystal surface. The deposited energy in this case is less than the original $\gamma$-ray energy and this event will increase the background and the information about the initial $\gamma$-ray energy would be lost. The anti-Compton shield has been invented to reduce the background.

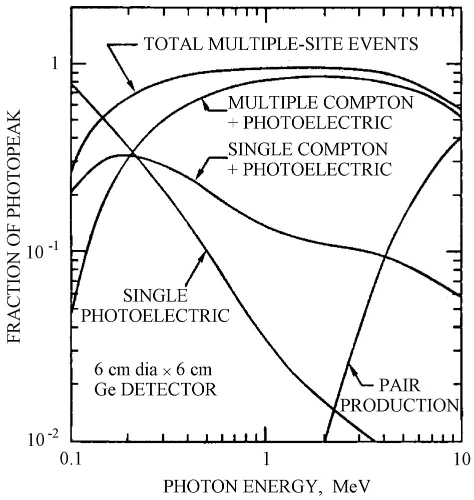


Fig. 7. Monte-Carlo simulations of the photoeffect, Compton effect, and pair production contributions in the full absorption peak (from [1]) made for coaxial high-purity Ge detector with dimensions $d = 6$ cm, $l = 6$ cm

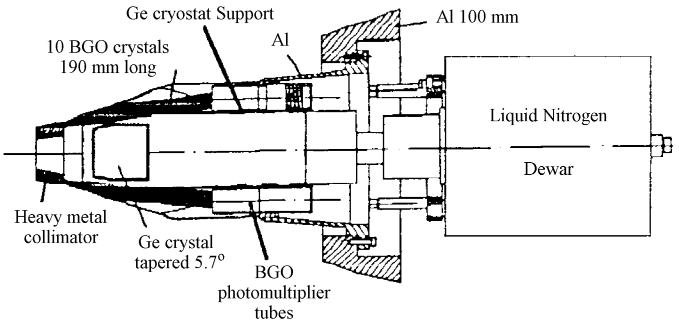


Fig. 8. Escape-suppressed spectrometer

High resolution escape-suppressed spectrometer (ESS) (see Fig. 8) consists of a Ge detector surrounded by a scintillator detector to detect and reject the scattered radiation from the Ge crystal [7]. These scintillators are optically isolated, each with PM tube, and protected by heavy metal collimators from the direct $\gamma$-radiation. In detector systems with spatial limitation this anti-Compton shield is made of scintillator crystals of BGO ($Bi_4Ge_3O_{12}$) in order to achieve maximum probability of photon detection for minimum detector volume. BGO has high efficiency because of the large $Z = 83$ of Bi.

The BGO shield reduces effectively the background. If the scattered $\gamma$-ray enters one of the BGO detectors this event will be suppressed by a veto signal from the escape-suppression shield.

The $P/T$ ratio of the large Ge detectors in EUROBALL detector array has been determined for the $^{60}$Co spectrum and it has been found 0.25 without and 0.65 with escape-suppression [6].

## 4. COMPOSITE DETECTORS

In order to increase the detection efficiency composite detectors have been developed. They consist of several Ge detectors in a close-packed geometry and encapsulated, either together or separately, in a common escape-suppression shield and cryostat. The composite detector acts as one large detector and it has higher efficiency than a single Ge detector (Fig. 5). When a Compton scattered $\gamma$-ray does not enter a BGO crystal but a neighbouring Ge crystal and it stops in it, its initial energy could be restored by summing the energies deposited in both Ge crystals (sec. 5.1). This procedure will increase the detection efficiency of a spectrometer with several Ge crystals. The composite detector can also increase the detector array granularity thus reducing the Doppler broadening typical for large size detectors.

Two types of composite detectors have been developed for EUROGAM2 and EUROBALL projects: *clover* (Fig. 9, left) and *cluster* (Fig. 9, right) detectors. They consist of several Ge crystals mounted in a common cryostat and a common escape-suppression shield [8, 9].

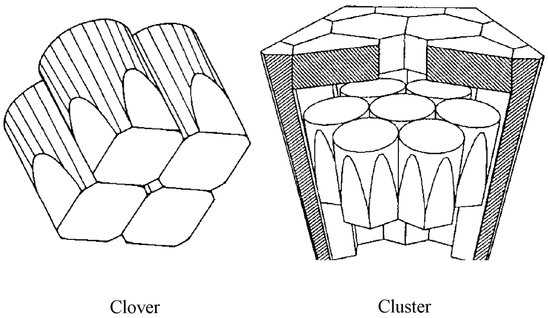


Fig. 9. Two types of composite detectors used in EUROBALL multidetector array (from [10])

- The clover detector consists of 4 independent Ge crystals packed together like a four-leaf clover [4, 9]. The clover individual crystals are smaller than those of the large Ge detectors. In EUROBALL detector array they are placed at 90° to the beam direction where the Doppler broadening due to the crystal opening is the largest.

- The cluster detector consists of 7 semi-hexagonal tapered detectors separately encapsulated. The encapsulating technology offers advantages for easy changing of one or more crystals in the cluster in case of irradiation damage. The space between two neighbouring crystals is only 2.5 mm. The cluster spectrometers have an additional BGO shield on the rear side consisting of 6 BGO crystals. Fig. 9 (right) shows a schematic view of a cluster detector with its ESS crystals.

## 5. COMPOSITE DETECTOR EFFICIENCY

The total photopeak efficiency of a composite detector $(\epsilon_p\omega)_t$ can be written as a sum over all $N$ detector efficiencies $(\epsilon_p\omega)_i$:

$$(\epsilon_p\omega)_t = \sum_{i=1}^{N}(\epsilon_p\omega)_i \tag{29}$$

It can be increased using the add-back procedure but when it is applied "phantom" peaks could appear in the spectra.

### ADD-BACK MODE

A composite detector with $N$ crystals will have an efficiency which is higher than the efficiency defined in eq. (29) if the add-back mode is applied.

Let us suppose that several crystals have been hit by one $\gamma$-ray which is Compton-scattered in all crystals with exception of the last one where it is absorbed by photoeffect [11]. The initial $\gamma$-ray energy could be restored by summing the energies deposited in each Ge crystals. Therefore the total composite detector efficiency will be

$$(\epsilon_p\omega)_t = \sum_{i=1}^{N}(\epsilon_p\omega)_i + \sum_{j=1}^{M}(\epsilon_p\omega)_j, \tag{30}$$

where $(\epsilon_p\omega)_i$ is the $i^{th}$ crystal efficiency, $(\epsilon_p\omega)_j$ is the photopeak efficiency of two and more Ge crystals fired simultaneously. $N$ is the number of the single crystals and $M$ is the number of combinations of two and more crystals. Obviously, the total efficiency obtained with eq. (30) is higher than the previous one defined by eq. (29):

The *summation factor* $F$ is defined as:

$$F = \frac{\sum\limits_{i=1}^{N}(\epsilon_p\omega)_i + \sum\limits_{j=1}^{M}(\epsilon_p\omega)_j}{\sum\limits_{i=1}^{N}(\epsilon_p\omega)_i}. \tag{31}$$

A single crystal has relative efficiency (see Table 1) of 20% for clovers and 59% for clusters. The relative efficiencies of these two composite detectors in add-back mode are 123% and 595%, respectively. So the summation factors for clover and cluster detectors are respectively 1.54 and 1.44 for a $\gamma$-ray of 1.33 MeV.

**Table 1.** Some characteristics of Ge detectors of EUROBALL 4: number of spectrometers of each type ($N$); total number of individual crystals for each type ($N_{\mathrm{cr}}$) and their dimensions – diameter ($d$) and length ($l$); distance from the detect or front surface to the target ($D$); crystal relative efficiency $(\epsilon_p\omega)_i$, whole spectrometer efficiency $(\epsilon_p\omega)_t$ (with add-back mode applied), number of BGO surrounding crystals ($N_{\mathrm{BGO}}$) in each suppression shield

| detector type | $N$ | $N_{\mathrm{cr}}$ | $d$, mm | $l$, mm | $D$, cm | $(\epsilon_p\omega)_i$ | $(\epsilon_p\omega)_t$ | $N_{\mathrm{BGO}}$ |
|---|---|---|---|---|---|---|---|---|
| Ge tapered | 30 | 30 | 70 | 75.85 | 37 | 70 % | 70 % | 10 |
| clovers | 26 | 104 | 50 | 70 | 29.5 | 20 % | 123 % | 12 |
| clusters | 15 | 105 | 70 | 78 | 45 | 59 % | 595 % | 18 |

### PILE-UP SUMMING

Highly excited nuclei at high spin usually emit over 30 $\gamma$-rays ($M_\gamma \cong 30$) and several neutrons ($M_n = 5$ to 6) in cascade within the detector resolving time, i.e. in coincidence. A finite probability exists that more than one $\gamma$-ray may hit a detector in the same event. In this case true coincidence summing happens and the output pulse height corresponds to the sum energy of all $\gamma$-rays detected in a single Ge detector. A new peak corresponding to the sum energy appears that does not exist in the decay scheme. This is known as *true coincidence "phantom" peak.* The relative contribution of the true coincidence sum peaks depends on the decay scheme and the detector efficiency and not on the detector counting rate. However, some summing effects also appear in the case of high counting rate. Such events are known as pile-up summing, to distinguish from the true coincidence summing. In a pile-up event, two or more uncorrelated events occur so close in time that their respective pulses give one single pulse in the detection system. A new *pile-up "phantom" peak* appears. These true coincidences and pile-up summing effects increase when the add-back mode is applied, which reduce the real peak areas. The choice of the add-back procedure for all composite detectors, complicated by these summing effects, will be discussed below.

## 6. THE EUROBALL 4 MULTIDETECTOR ARRAY

### GEOMETRY

The European multidetector array EUROBALL [5] consists of 239 germanium (Ge) crystals mounted in 71 ESS [12, 9] (Fig. 10). At present the EUROBALL detector array is located on a beamline of the VIVITRON accelerator at IReS, Strasbourg, France.

The EUROBALL $\gamma$-ray multidetector system contains 26 Clover spectrom-

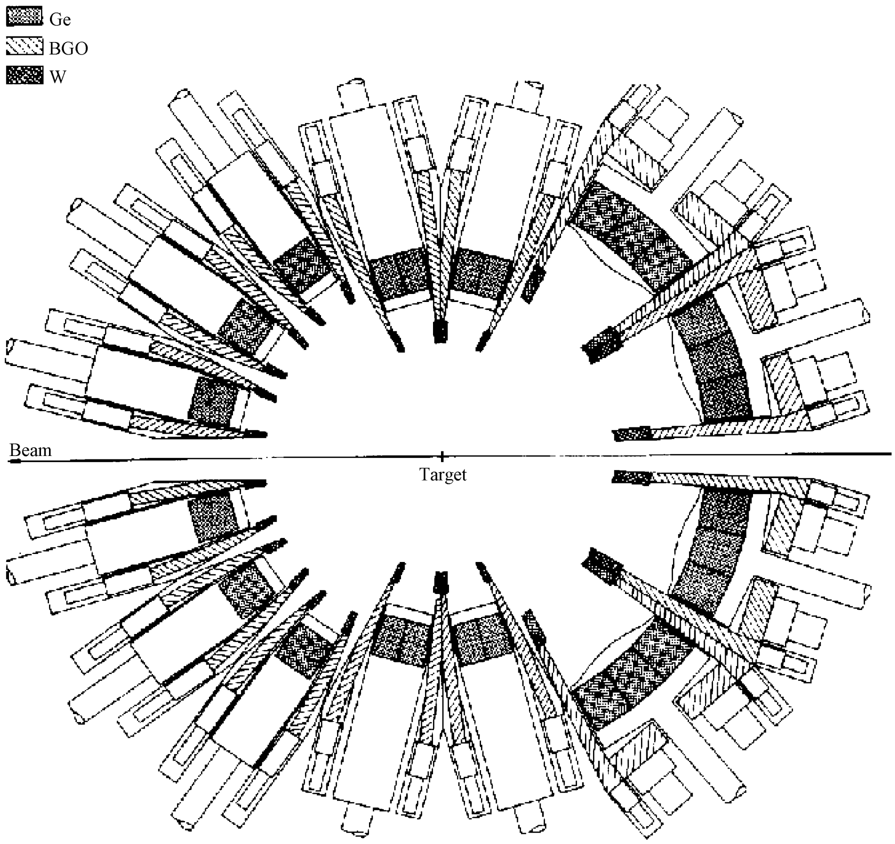


Fig. 10. Cross section of EUROBALL4 (from [10])

eters in two rings close to $90^0$ with respect to the beam direction, 15 Cluster spectrometers placed in the backward quadrant and 30 individual Ge detectors in the forward quadrant. The main features of EUROBALL are presented in Table 1.

## DATA AQUISITION SYSTEM

Each Ge detector unit contains a pre-amplifier, which function is to amplify weak signals from the detector. The signals from Ge pre-amplifiers and BGO phototubes enter their respective VXI cards: Ge card, BGO card, Clover card, Cluster card and BGO Cluster card.

1. Ge card. The Ge card contains 6 identical processing channels, one of them is shown in Fig. 11. Each channel accepts signals from one Ge pre-amplifier. The signal is led to Timing Filter Amplifier (TFA) and Dual gain pulse shaper.

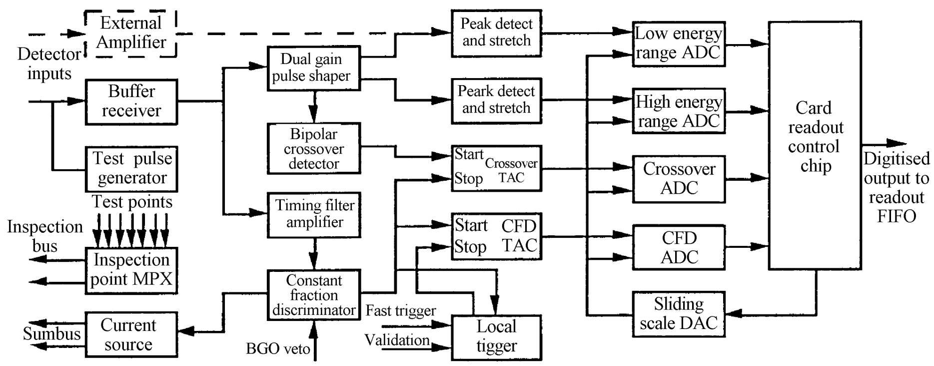


Fig. 11. Block diagram of a single Ge signal processing in a VXI card (from [13])

Constant Fraction Discriminator (CFD) treats the signals from TFA. The time the CFD fires, there is a programmable delay after which a pulse with fixed width enables the channel's sumbus driver to put 1 mA current onto the sumbus. The width of this pulse defines the time window constituting a *single event.* The Master Trigger (MT) card [14] examines the sumbus. The MT generates a Fast Trigger (FT) signal if enough detectors are hit simultaneously. The number of fired detectors is programmable. If the number of fired detectors is not equal to the required number then MT would not liberate FT signal and Local Trigger (LT) will reset itself. The channel would look for the next event.

The validation comes fixed time after FT. The validation signal is used by the LT section to enable readout of the digitized event. Non arrival of the validation signal makes the readout to be abandoned.

The CFD starts also time to amplitude converter (TAC). The LT, which accepts a fast trigger and validation signals from the master trigger, stops the TAC. So the TAC module makes a signal with amplitude proportional to the time interval between "Start" and "Stop" signals from the Trigger and CFD.

Additional timing information from a second Crossover TAC, started from the CFD output signal, but stopped at the crossover point of a bipolar pulse formed in the Bipolar Crossover detector. This information could be useful for the pile-up rejection in the event builder.

The signals from both TAC and from both Peak Detector and Stretchers are provided to 4 amplitude to digital converters (ADC) where the amplitudes of the analog pulses are digitized. They emit 4 output signals: low energy range (4 MeV); high energy range (20 MeV), peak time TAC and CFD to fast trigger TAC. The ADCs have 13 bits resolution (8k channels).

2. BGO card. The signals of each 10 element shields are summed. Apart from this basic difference the processing chain on a BGO channel is very similar to the Ge channel processing. One energy range is provided 0–20 MeV at 10 keV per increment, requiring only 11 bits precision from the ADC. There are total of 6 VXI BGO cards.

3. Clover card. There are 26 cards. Each card has 4 Ge channels plus one spare Ge channel plus 1 BGO channel. After signal processing of the inputs from Ge detectors and BGOs the output signals from this card contain information on energy, timing and hit pattern.

4. Cluster card. Each card has 7 channels plus 1 spare channel (2 energy + 1 timing parameters per channel)

5. BGO Cluster card. Each card has 18 channels plus 1 spare channel (energy and timing parameters per channel) and 1 "sum" channel (3 parameters)

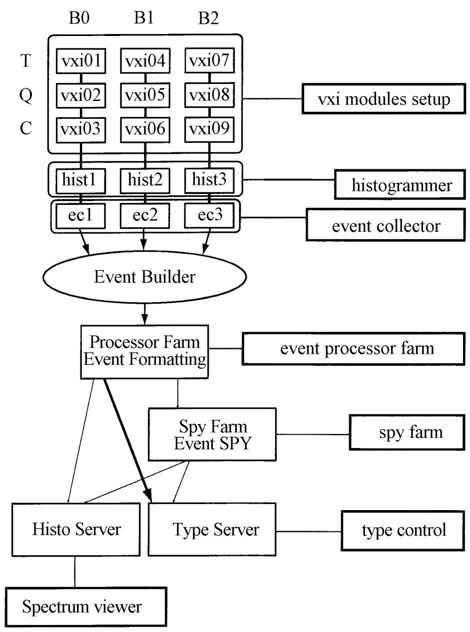


Fig. 12. EUROBALL data acquisition system (from [9])

All VXI cards for the escape suppressed Ge detectors are mounted in 9 VXI crates, labelled VXI01 to VXI09 (Fig. 12). The data stored in each crate readout card are transfered through DT32 bus to a *Hardware Histogramming Unit* (HHU).

This unit is software programmable to select any specific parameters from any chosen detector and to build histograms (spectra). The histograms can be examined using a workstation to check the data quality and monitor detector performance. The spectra built with this unit give the data before super-event construction. The 3 V.M.E. modules, named Event Collector (EC), accept the event fragment from the 3 DT32 busses. The Event Builder (EB) has several functions: to check the event fragments and the quality of the raw data from the EC; to remove the fragment tokens and to form the complete event in a more compact format than the raw data. All data sources (ROCO) are required to generate an event fragment even if it contains no data. This is important for the event construction since it is possible to detect a missing event fragment or malfunctioning data source which would not be the case if empty fragments were not required.

The super event building and online analysis take place within the Processor Farm (PF), which consists of commercially available workstations. The super events are sent to the Tape Server (TS). The workstations have some programs allowing fast access to the data acquisition process: Event Spy, Tape Server and Histogram Server. The event processing is performed by the *Event Spy Farm* (ESF). The ESF accepts complete event as input, producing both formatted data, which are sent to the *Tape Server* (TS), and spectra sending to the *Histogram Server* (HS), which allows the online storage of pre-sorted spectra. In this way, the user can check the validity of the acquired information.

The super events are usually recorded on DLT cassettes with a capacity of 40 Gb. The exact type of the data words written on the tape is specified by the user, but generally each event is written as a group containing the following information:

i) fold of the event (number of detectors fired);
ii) detector identification number;
iii) 4 MeV scale energies;
iv) 20 MeV scale energies;
v) timing information.

## ENERGY CALIBRATION

The signal amplification is different for each processing channel. In order to unify them for all detectors the following procedure is applied.

One Ge detector that has good counting rate and resolution during the experiment is selected as a reference detector. The spectra of all other Ge detectors have to be renormalized linearly to it.

In order to keep good resolution:

1. If the alignment function of a Ge detector is linear only in some part of the whole energy range, then the nonlinear part has to be cut off.

2. If a detector has totally nonlinear alignment function its information is not taken into account.

Moreover, the amplification in a processing channel can change during the experiment. To control this change, experimental spectra corresponding to successive runs containing small part of the whole data are built. The alignment parameters have to be found for each run.

After such a procedure, called gainmatching, all Ge detectors will have similar behaviour and the multidetector array will work as one spectrometer. This procedure was made with the program GAIMATCH [15].

The spectra from all properly working detectors have to be added and the energy calibration function $E = f(channel)$ can be found using peaks with known energy.

**Table. 2.** 19 configurations in a hit Cluster detector. The first 12 spectra are built with add-back mode. Spectra 13 and 14 are obtained without add-back. The symbols in the column "Configuration" correspond to the drawings of Fig. 13. The spectra 15 and 17 are built from the single crystal and 16 and 18 are made from the 2 and 3 adjacent crystals, respectively, where the add-back mode was used

| Configuration number | Configuration | Mode |
|---|---|---|
| 1 | 1 | |
| 2 | 2 | with add-back |
| 3 | 3 | with add-back |
| 4 | 4 | with add-back |
| 5 | 5 | with add-back |
| 6 | 6 | with add-back |
| 7 | 7 | with add-back |
| 8 | 1+1 | with add-back |
| 9 | 1+1+1 | with add-back |
| 10 | 1+2 | with add-back |
| 11 | 1+3 | with add-back |
| 12 | 2+2 | with add-back |
| 13 | 1+1 | without add-back |
| 14 | 1+1+1 | without add-back |
| 15–16 | 1+2 | add-back only for the 2 adjacent crystals |
| 17–18 | 1+3 | add-back only for the 3 adjacent crystals |
| 19 | 2+2 | add-back only for the adjacent crystals |

## 7. EXPERIMENTAL STUDY OF CLUSTERS' ADD-BACK MODE

To study the behavior of the composite Cluster detector over a wide energy range the spectra of $^{60}$Co source and $^{56}$Co have been analyzed [16].

In order to increase the multidetector efficiency at high energies the add-back procedures have to be studied experimentally. The problem is to determine, when

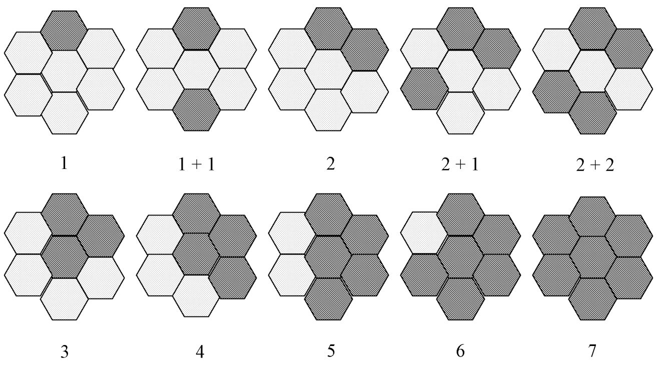


Fig. 13. Some cluster configurations

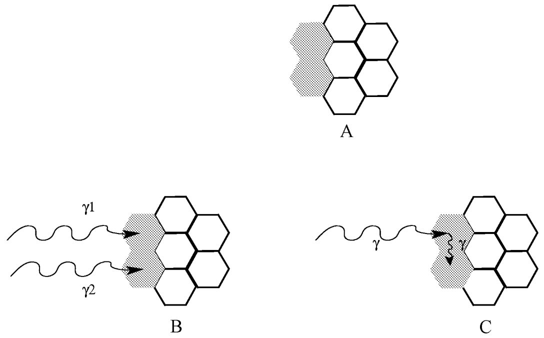


Fig. 14. Pile-up effects and Add-back mode in a composite detector

more than one crystal are hit in a cluster spectrometer (Fig. 14 A), whether this is one Compton scattered $\gamma$-ray (Fig. 14 C), or several $\gamma$-rays hit the crystals in coincidence (Fig. 14 B)? To answer this question 19 spectra have been constructed by means of the code Fantastic [17]. These spectra correspond to 19 possible configurations of the hit cluster crystals (defined in Table 2): config. 1 to 7 are for $1, 2, \ldots, 7$ hit crystals in coincidence with add-back mode. The other configurations are various possible combinations of 2, 3 and 4 hit crystals with and without add-back for the cluster structure of 7 crystals shown in Fig. 13, i.e. $1+1$ means two not adjacent crystals hit in coincidence, $1+2$ means one separate and two adjacent crystals hit in coincidence, etc.

The full absorption peak in config. 1 comes from photoeffect or multiple Compton scattering with photoeffect at the end of its trajectory in the same crystal.

By applying add-back procedure we suppose that this event corresponds to one $\gamma$-ray which is Compton scattered to the neighbouring crystal. The full absorption peak comes from multiple Compton scattering and photoeffect of the last scattered

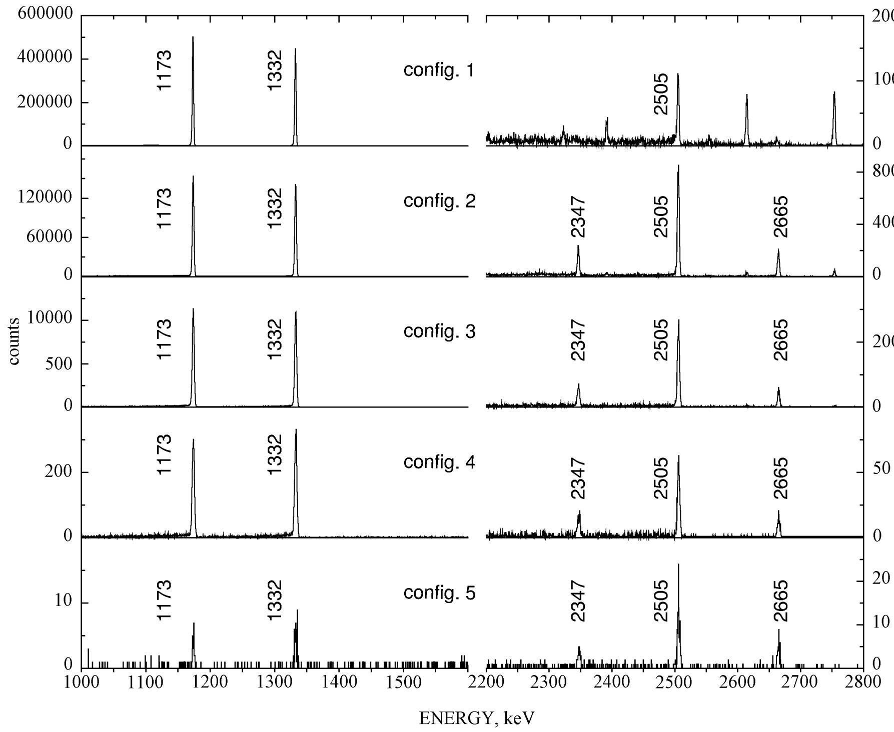


Fig. 15. The $^{60}$Co spectra for the first five configurations

$\gamma$-ray. Due to the increase of Compton scattering cross-section with energy, the configurations with more than one crystal hit in coincidence have to be investigated.

The spectra for configurations with more than one hit in coincidence crystal without add-back mode have also been constructed with the assumption that the crystals are hit by different $\gamma$-rays.

The code GF2 from the RADWARE code pack [18] has been used in the analysis of these spectra.

## $^{60}$Co SOURCE

The $^{60}$Co spectra for the first five configurations in a Cluster composite detector are presented in Fig. 15. The best statistics is for one and two crystals hit in coincidence. The probability for triple, quadruple, etc hits decreases rapidly, nearly by a factor of $10^5$ from 2 to 5 hit crystals.

The measured contribution of the first 4 configurations (1.33 MeV $\gamma$-ray) are presented in Table 3. One can see that over 70% of the $\gamma$ quanta of energy 1.33 MeV have given their energy in one Ge crystal. About 27% of them are Compton

**Table. 3.** Comparison of the measured in present work and measured in [10] contributions of 1.33 MeV $\gamma$-ray in the first 4 configurations

| Cluster | Measured in present work | Measured [10] |
|---|---|---|
| 1-det. response(%) | 70.4 | 69.4 |
| 2-det. response(%) | 27.1 | 27.1 |
| 3-det. response(%) | 2.4 | 3.3 |
| 4-det. response(%) | 0.1 | 0.2 |

scattered to the neighbouring crystal. The multiple Compton scattering through more than 2 crystals can be neglected. It can be seen that our values are in agreement with the experimental measured values obtained before our study [10]. The $P/T$ ratio (the peak $P$ area is the sum area of both $^{60}$Co $\gamma$-rays) as a function of configuration number is plotted in Fig. 16. This ratio is higher than 0.5 only for config. 1 to 4 (1, 2, 3 and 4 crystals hit in coincidence). The ratio decreases rapidly when 3 to 7 crystals are hit in coincidence and is about 0.1 for configuration 5. If all these spectra are added the sum spectrum will have lower ratio $P/T$. In order to keep $P/T \geq 0.5$ only the first 4 configurations should be used.

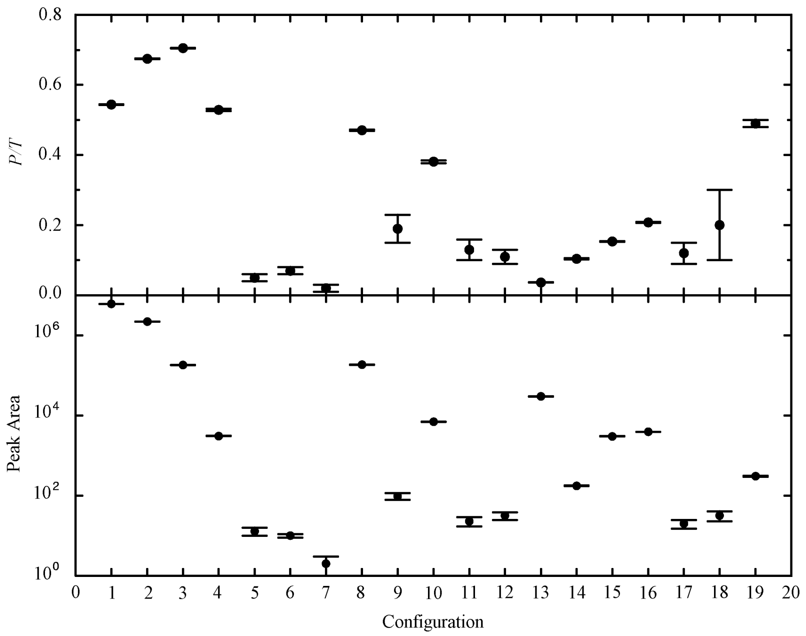


Fig. 16. $P/T$ ratio and peak areas in some cluster configurations

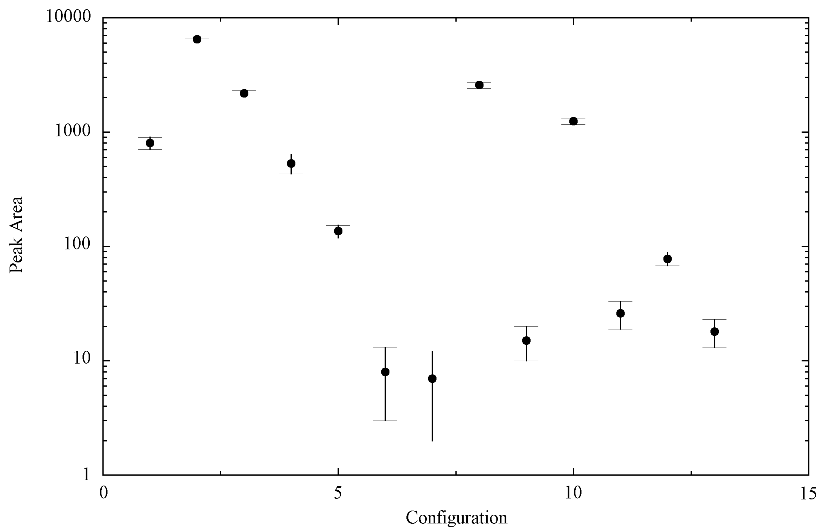


Fig. 17. The phantom peak ($E_1 + E_2 = 2505$ keV) area for $^{60}$Co, measured in the spectra from the first 12 configurations (Table 2)

The $^{60}$Co disintegration scheme has only two $\gamma$-rays in cascade, therefore the peaks at energies 2346.5 keV, 2665.0 keV and 2505 keV do not exist in the $^{60}$Co disintegration. The first two of them can be attributed to the the pile-up effects $2\times E_1$=2346.5 keV, $2\times E_2$=2665.0 keV and the third one is due to the true coincidence events $E_1 + E_2$=2505 keV (see sec. 5). The highest values of this "phantom" peak (as seen in Fig. 17) are for double and triple coincidences between adjacent crystals with add-back but its area is only 0.1% of the main $\gamma$-rays peak areas. It also can be seen in Fig. 17 that the "phantom" peak area jumps for config. 8 (1+1) and 10 (1+2), where add-back mode is applied. The other two "phantom" peaks show the same behaviour.

In the case of nuclear reaction the probability of "phantom detection" will increase with the number of crystals included in the add-back mode, due to the increased multiplicity ($M_\gamma \cong 30$).

## $^{56}$Co SOURCE

To prove the role of the multiple Compton scattering at higher energies the set of 19 spectra for $^{56}$Co has been studied. These spectra for several configurations are presented in Fig. 18.

The number of counts and $P/B$ ratio decrease when the configuration number increases from 1 to 4. Config. 5, 6, 7 are not shown as they are empty. The comparison between configs. 2 and 8(1+1) shows that the $P/B$ ratio is low for config. 8(1+1).

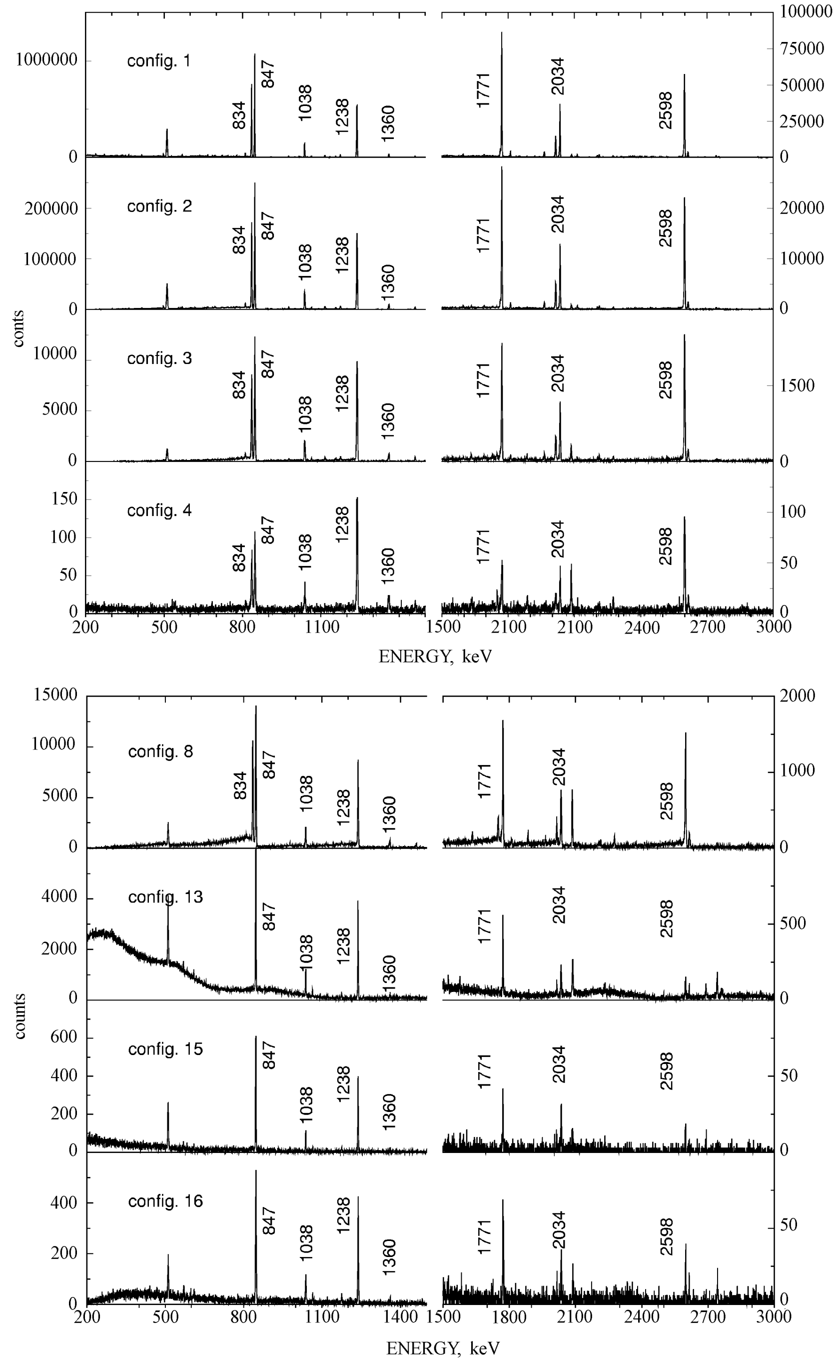


Fig. 18. The $^{56}$Co spectra for several configurations

It can be seen in Fig. 18 that the high energy peak areas increase relatively to the low energy peak areas when 2, 3 and 4 crystals with add-back contribute (confs. 2 to 4). In order to account for the different $\gamma$-ray intensities we have to introduce a new relative efficiency defined as:

$$\epsilon'_{\rm rel}(E_\gamma) = \frac{N_{\rm ph}}{I_{\rm rel}} \tag{32}$$

where $N_{\rm ph}$ is the full absorption peak area, $I_{\rm rel}$ is the relative intensity taken from a nuclear data reference book, i.e. [19]. Table 4 shows the ratio $\epsilon'_{\rm rel}(E^i_\gamma)/\epsilon'_{\rm rel}(847)$, where $i$-th energy efficiency and 847 keV efficiency are for the same configuration.

Two conclusions should be drawn from the results shown in Table 4:

1. This ratio decreases with energy for configs. 1 and 2. Config. 1 is twice less effective for a 3451 keV $\gamma$-ray than for a 847 keV $\gamma$-ray. The ratio increases with energy for configs. 3 and 4.

2. For fixed energy the ratio increases with the number of crystals included. Even for a 1038 keV $\gamma$-ray config. 4 is more effective than for the 847 keV $\gamma$-ray, which demonstrates the essential role of Compton scattering effect in this energy region.

**Table 4.** The relative efficiency relative to 847 keV efficiency for 4 configurations

| | config.1 | config.2 | config.3 | config.4 |
|---|---|---|---|---|
| $\epsilon'_{\rm rel}(1038)/\epsilon'_{\rm rel}(847)$ | 0.93 | 1.03 | 1.18 | 1.67 |
| $\epsilon'_{\rm rel}(1238)/\epsilon'_{\rm rel}(847)$ | 0.82 | 0.97 | 1.29 | 2.22 |
| $\epsilon'_{\rm rel}(1771)/\epsilon'_{\rm rel}(847)$ | 0.62 | 0.81 | 1.48 | 3.67 |
| $\epsilon'_{\rm rel}(2034)/\epsilon'_{\rm rel}(847)$ | 0.56 | 0.81 | 1.40 | 4.89 |
| $\epsilon'_{\rm rel}(2598)/\epsilon'_{\rm rel}(847)$ | 0.48 | 0.74 | 1.53 | 6.44 |
| $\epsilon'_{\rm rel}(3253)/\epsilon'_{\rm rel}(847)$ | 0.42 | 0.68 | 1.64 | 22.78 |
| $\epsilon'_{\rm rel}(3451)/\epsilon'_{\rm rel}(847)$ | 0.41 | 0.67 | 2.07 | |

These effects could be explained with the increasing of cross-section for Compton scattering with energy. The detector volume is more effective for $\gamma$-rays of energy 847 keV then for $\gamma$-rays of higher energies. The ratio $\epsilon'_{\rm rel}(E)/\epsilon'_{\rm rel}(847)$ increases with the number of Ge crystals included in add-back procedure, due to the multiple Compton scattering cross-section increasing with energy.

The increase of the Compton scattering cross-section with energy leads to an increasing of the add-back factor $F$ with energy. This dependence is shown in Table 5. The add-back between two neighbouring crystals was made.

It has to be noted that in the spectra shown in Fig. 18 there is a peak of energy 834 keV, which does not exist in the $^{56}$Co disintegration scheme. It disappears in spectra of configs. 13, 15 and 16 where no add-back mode is applied. This transition probably belongs to the $^{54}$Mn disintegration scheme. This peak appears in first 4 configurations (and config. 8) because when the 834 keV $\gamma$-ray penetrates into the cluster it may hit several single crystals and when an add-back was made

**Table 5.** Summation factor $F$ and the relative efficiency as a function of energy

| Energy, keV | 847 | 1037 | 1238 | 1771 | 2034 | 2598 | 3253 | 3452 |
|---|---|---|---|---|---|---|---|---|
| $F$ | 1.31 | 1.34 | 1.37 | 1.42 | 1.44 | 1.50 | 1.54 | 1.57 |
| $\epsilon_{\rm rel}$ | 541 | 553 | 566 | 586 | 595 | 620 | 636 | 648 |

between these crystals its total energy will be restored. This peak disappears in configurations without add-back, where it is supposed that the different crystals are hit by different $\gamma$-rays. Really, this peak does not exist in the spectrum for config. 13.

The peak of energy 834 keV could appear in spectrum of config. 13 if both crystals are hit simultaneously by two different $\gamma$-rays one of which is the $\gamma$-ray of energy 834 keV. It could happen in two cases:

i) in case of high counting rate.

ii) when $\gamma$-ray of energy 834 keV is emitted in coincidence with another $\gamma$-ray which could be detected.

The counting rate in case of $^{60}$Co is high enough for observation of accidental ("pile-up") coincidences (prev. paragraph) but it is not the case of $^{56}$Co source. The $\gamma$-ray of energy 834 keV would be detected with the $\gamma$-ray of energy 847 keV, for example, if the counting rate was high. The pile-up summing peak of 847 keV (most intensive transition in $^{56}$Co) + 834 keV ($^{54}$Mn)=1681 keV is not observed in the spectrum of config. 1.

$^{56}$Co source emits $\gamma$-ray of energy 847 keV in coincidence with other $\gamma$-rays which are detected (see. Fig. 18, spectrum from config. 13). The $\gamma$-ray of energy 834 keV is not emitted in coincidence with other $\gamma$-ray that could be detected.

One can conclude that the peak of energy 834 keV disappears in spectra from configs. 13, 15 and 16 due to the low counting rate and the fact that the $\gamma$-ray of energy 834 keV is not emitted in coincidence with another $\gamma$-ray that could be detected.

## CONCLUSIONS ON THE CLUSTER ADD-BACK STUDY

Our analysis on the cluster add-back procedures in different configurations shows that:

1. The major part of the statistics is from single (Clu1) and double hits with add-back mode (Clu2).
2. The highest P/T value is for the first 2 configurations.
3. "Phantom" peaks appear when the add-back mode is applied.

In order to restrict this effect and to keep $P/T \geq 0.5$ the add-back mode has to be made only for two adjacent crystals. With these two configurations, denoted as Clu1 and Clu2, we can restore effectively the whole photon energy and the cluster detectors efficiency has a considerable increase at high energy.

Similar analysis for clover detectors was completed before our study. The measured contributions at 1.33 MeV of single (one crystal hit), double, triple, and quadruple hits (2, 3, and 4 crystals in coincidence) of the total clover detector efficiency are 67%, 30%, 3% and 0.1%, respectively [20].

## 8. EUROBALL EFFICIENCY CALIBRATION

Any measurement of $\gamma$-ray emission requires exact knowledge of the detector efficiency.

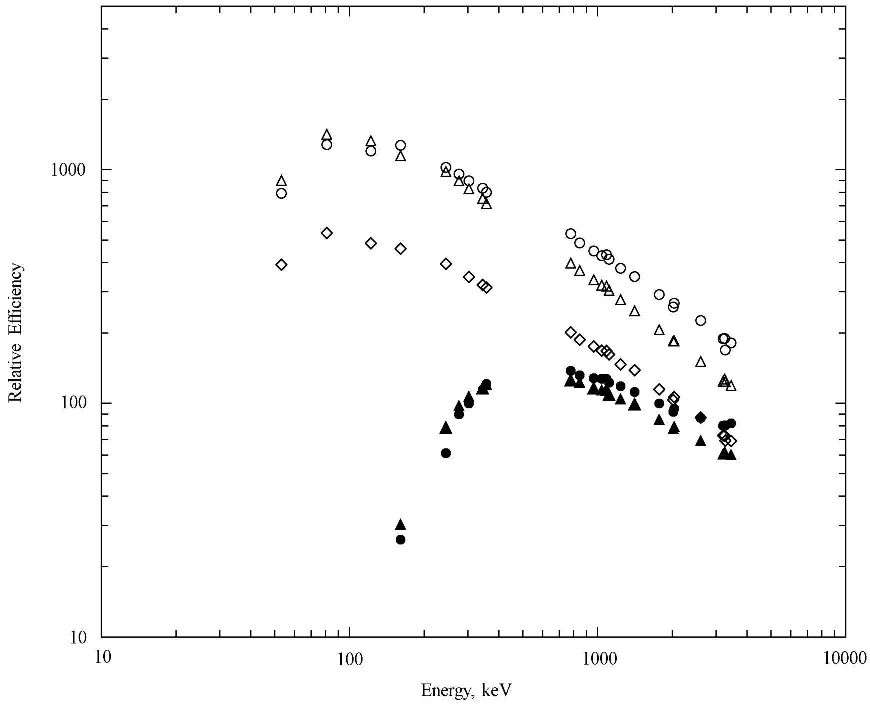


Fig. 19. The efficiencies of all clusters (open circles), all clovers (open triangles) for singles and for double hits with add-back (full circles and triangles for clusters and clovers, respectively) and for Ge-tapered detectors (open diamonds). The error-bars are less than the symbol size

The total absorption coefficient decreases with energy, therefore the efficiency of each Ge detector (and of the whole multidetector spectrometer) will also decrease. To determine the detector efficiency over a wide energy range, the following sources have been measured: $^{133}$Ba (8 peaks in the range 53–384 keV) and $^{152}$Eu (8 peaks in the range 122–1408 keV), $^{56}$Co (11 peaks in the range 847–3451 keV). Therefore the EUROBALL efficiency was obtained in the energy range between 53 keV and 3451 keV. After the energy calibration of all Ge crystals the sum spectra for several configuration (single Ge crystals and two neighbouring crystals in a

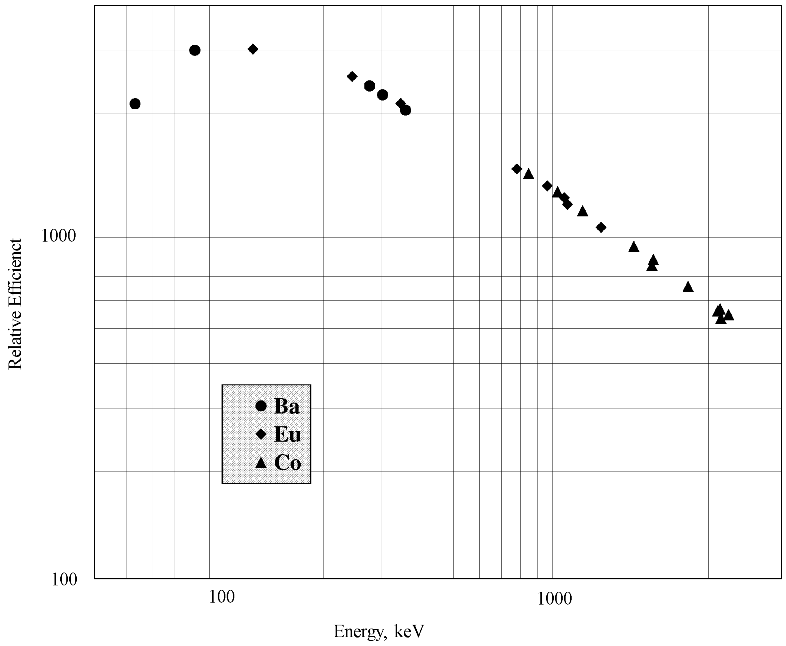


Fig. 20. The relative efficiency of EUROBALL detector array

composite detector with add-back) have been constructed for each source.

The efficiency curves obtained from the spectra of these three sources differ from each other due to the different counting time and activity.[1] As the energy ranges of these sources partly overlap we can adjust them by linear renormalisation multiplying by appropriate factors in order to obtain an unique efficiency function.

Comparison of the efficiencies of all detector types in EUROBALL are presented in Fig. 19: Ge tapered (open diamonds), clovers (open triangles) and clusters (open circles). The lower efficiency for Ge tapered detectors is due to the difference in the number of Ge crystals: only 30 against 104 and 105 for the composite detectors. The clover and cluster detectors have nearly equal efficiency in the low energy region. However, the cluster detector efficiency becomes higher from 800 keV on and at about 3 MeV it is twice that of the clover detectors. This behaviour can be explained by the crystal size.

The curves with full circles and full triangles are for double hits (with add-back) in the clusters (Clu2) and clovers (Clo2), respectively. The relative efficiencies

[1]Each source emits $N_{\rm em}$ $\gamma$-rays in counting time $\Delta t$:

$$N_{\rm em} = \Delta t A_0 e^{-(\ln 2)t/t_{1/2}}. \tag{33}$$

Here $t_{1/2}$ is the source half-life time, $t$ is the time since the source production, and $A_0$ is its initial activity. As $N_{\rm em}$ and $N_{\rm ph}$ ($\sim N_{\rm em}$) depend on $\Delta t$, $A_0$ and $t$, then $\epsilon_{\rm rel}$ depends also on them.

of clusters and clovers in add-back mode (Clu2 and Clo2) are less than their respective single crystal relative efficiencies (Clu1 and Clo1) in the low energy region, because the photoeffect is dominant there. The probability of Compton scattering increases with energy, so in add-back mode the relative efficiency of the Clu2 becomes higher than that of the Clo2 above 800 keV and at 3 MeV it is nearly equal to the clover detectors efficiency with one hit crystal. Such a behaviour reveals the high performance of the cluster detectors at high energies.

The whole efficiency of EUROBALL can be obtained from the sum spectrum of all individual detectors plus the composite detectors add-back spectra and it is presented in Fig. 20.

Due to the creation of pairs $e^-e^+$ (see sec. 1) the detector efficiency decreases more rapidly for $\gamma$-rays with $E_\gamma > 1.022$ MeV. Therefore on log-log scale the efficiency curve will have two linear parts: the first one is from $\sim$ 220 keV to $\sim$ 1.022 MeV and the second one is above 1.022 MeV. The relative efficiency in these two energy ranges can be calculated by the following expressions:

$$\epsilon'_{\mathrm{rel}}(E_\gamma) = 10^{4.655} E_\gamma^{-0.524} \qquad 220 \text{ keV} < E_\gamma < 1.022 \text{ MeV} \tag{34}$$

$$\epsilon'_{\mathrm{rel}}(E_\gamma) = 10^{5,034} E_\gamma^{-0.649} \qquad E_\gamma > 1.022 \text{ MeV} \tag{35}$$

## 9. CONCLUSIONS

This work presents an experimental study of the EUROBALL Cluster detectors. It is related to the most important problem of their application in the large multidetector arrays: how to treat the coincidences between their seven crystals.

Our analysis of the spectra for different Cluster configurations, of the "phantom" peaks and the efficiencies of the EUROBALL detectors allows to draw the following conclusions:

i) Due to the appearance of "phantom" peaks the recommended add-back procedure is to use only two adjacent Cluster crystals. Moreover, the major part of the statistics is from single and double hits with add-back mode. So in these configurations we can restore effectively the whole photon energy.

ii) The total efficiencies of the EUROBALL Cluster, Clover and Tapered detectors are obtained and compared with each other. It was shown that the Cluster detectors efficiency has considerable increase at high energies (>600 keV).

REFERENCES

1. Knoll, G. Radiation Detection and Measurements. John Wiley and Sons, Second edition, 1989.
2. Leo, W. R. Techniques for Nuclear and Particle Physics Experiments. Springer-Verlag, Second edition, 1994.
3. Krane, K. Introductory Nuclear Physics. John Wiley and Sons, 1988.
4. de France, G. Thése de doctorat. ULP, Strasbourg 1991.
5. Gerl, J. and Lieder, R. M. EUROBALL III Proposal. GSI Darmstadt Report, 1992.

6. Nolan, P. J., F. A. Beck, and D. B. Fossan. *Annu. Rev. Nucl. Part. Sci.*, **45**, 1994, 561.
7. Twin, P. J. et al. *Nucl. Phys. A*, **409**, 1983, 343.
8. Eberth, J. et al. *Nucl. Instrum. Methods Phys. Res. A*, **369**, 1996, 135.
9. EDOC's http://npg.dl.ac.uk/Euroball/documents/.
10. Lieder, R. New generation of gamma-detector arrays, *Experimental Techniques in Nuclear Physics*, Eds. Poenaru D. N. and Greiner W. Berlin, New York, Walter de Gruyter, 1997.
11. Haas, B. Multicompteurs $4\pi\gamma$ de grande rèsolution en ènergie, CRS, IN2P3-CNRS/Université Louis Pasteur, Strasbourg.
12. Simpson, J. *Z.Phys. A*, **358**, 1997, 139.
13. McPherson, at al. *IEEE Transition on Nuclear Science*, **39**, 4, 1992, 886.
14. Lazarus, I. *IEEE Transition on Nuclear Science*, **39**, 5, 1992, 1352.
15. Bauchet, A. Thèse de doctorat. UPS, Orsay, 2001.
16. Lalkovski, S. et al. Proc. of the Second Int. Balkan School on Nuclear Physics, Bodrum, Turkey (Sept. 10–15, 2000), *Balkan Phys. Letts./special issue*, 2000, 252.
17. Deloncle, I., M.-G. Porquet, and Dziri-Marcé. *Nucl. Instrum. Methods Phys. Res. A*, **357**, 1995, 150.
18. Radford, D. C. *Nucl. Instrum. Methods Phys. Res. A*, **361**, 1995, 297.
19. Firestone, R. Table of Isopopes, 8th edition, John Wiley inc. New York.
20. Kaci, M. Thèse de doctorat, UPS, Orsay, 1996.

Stephane Lalkovski
St. Kliment Ohridski University of Sofia
Faculty of Physics
Department of Atomic Physics
5 James Bourchier Blvd.
BG-1164 Sofia, Bulgaria
E-mail: stl@phys.uni-sofia.bg

*Received March 2003*